

Shellflow. I. The Convergence of the Velocity Field at 6000 km s^{-1}

Stéphane Courteau^{1,6}, Jeffrey A. Willick^{2,6}, Michael A. Strauss^{3,6}, David Schlegel^{5,3,6}, and
Marc Postman^{5,6}

- (1) NRC/Herzberg Institute of Astrophysics, Victoria, BC, and
University of British Columbia, Vancouver, BC
- (2) Deceased. Formerly at Stanford University, Department of Physics, Stanford, CA
- (3) Princeton University Observatory, Princeton, NJ
- (4) Durham University, Department of Physics, South Durham
- (5) Space Telescope Science Institute, Baltimore, MD
- (6) Visiting Astronomer, Kitt Peak National Observatory and Cerro Tololo
Inter-American Observatory

Epitaph for Jeffrey Alan Willick (October 8, 1959 - June 18, 2000)

We would like to dedicate this paper to the memory of our friend and collaborator Jeff Willick who died tragically a week after our paper was accepted for publication. The world of astronomy lost a superb scientist; we also lost a very dear friend. We will miss him deeply.

ABSTRACT

We present the first results from the Shellflow program, an all-sky Tully-Fisher (TF) peculiar velocity survey of 276 Sb–Sc galaxies with redshifts between 4500 and 7000 km s^{-1} . Shellflow was designed to minimize systematic errors between observing runs and between telescopes, thereby removing the possibility of a spurious bulk flow caused by data inhomogeneity. A fit to the data yields a bulk flow amplitude $V_{\text{bulk}} = 70_{-70}^{+100} \text{ km s}^{-1}$ (1σ error) with respect to the Cosmic Microwave Background, i.e., consistent with being at rest. At the 95% confidence level, the flow amplitude is $< 300 \text{ km s}^{-1}$. Our results are insensitive to which Galactic extinction maps we use, and to the parameterization of the TF relation. The larger bulk motion found in analyses of the Mark III peculiar velocity catalog are thus likely to be due to non-uniformities between the subsamples making up Mark III. The absence of bulk flow is consistent with the study of Giovanelli and collaborators and flow field predictions from the observed distribution of IRAS galaxies.

Subject headings: cosmology — large-scale structure — spiral galaxies

1. Introduction

It is of great cosmological importance to identify the volume of space, centered on the Local Group, which is at rest with respect to the Cosmic Microwave Background radiation (CMB). Very large-scale density fluctuations are required to move large volumes of galaxies in the gravitational instability picture of structure formation. In standard Cold Dark Matter (CDM) cosmogonies, density fluctuations on scales $\gtrsim 100h^{-1}$ Mpc are very small. As a result, the volume of space encompassed by the nearest superclusters (Great Attractor, Pisces-Perseus, Coma) is expected to be nearly at rest with respect to the CMB, and the distribution of matter *within* this volume should explain the $\sim 600 \text{ km s}^{-1}$ motion of the Local Group in the CMB frame. However, the detection of a large amplitude flow ($V_{\text{bulk}} \gtrsim 700 \text{ km s}^{-1}$) out to $15,000 \text{ km s}^{-1}$ by Lauer & Postman (1994), along with recent measurements of similar amplitude (although different directions) by Willick (1999b) and Hudson et al. (1999), have challenged the notion that the bulk flow on large scales is small, and are pushing CDM models to the breaking point (e.g., Feldman & Watkins 1994; Strauss et al. 1995). However, Giovanelli et al. (1998a,b) and Dale et al. (1999) find results consistent with no flow in their survey of field and cluster spirals out to $20,000 \text{ km s}^{-1}$.

The measured bulk flow on smaller scales is also controversial. The most recent POTENT reconstructions (Dekel et al. 1999) of the Mark III velocities (Willick et al. 1997; Mark III) find a bulk velocity within 6000 km s^{-1} of $370 \pm 110 \text{ km s}^{-1}$ in the CMB frame towards Supergalactic $(L, B) = (165^\circ, -10^\circ)$ ¹. Dekel et al. (1999) argue that this motion is generated by the *external* mass distribution on very large scales (see also Courteau et al. 1993). On the other hand, Giovanelli et al. (1998) find a flow consistent with zero on similar scales from their field sample, a result consistent with the surface brightness fluctuation data of Tonry et al. (2000) and SN Ia distances (Riess 2000).

Accurate ($\lesssim 150 \text{ km s}^{-1}$) measurement of the bulk flow at 6000 km s^{-1} requires that the galaxy distance data be homogeneous and free of systematic effects at the 2 – 3% level. This cannot be guaranteed for datasets, such as the Mark III catalog, that are composed of two or more independent peculiar velocity surveys. Indeed, Willick & Strauss (1998) found evidence of systematic errors in the relative zero points of the various TF samples that make up the Mark III catalog. Thus, the controversy over the observed bulk flow within $60h^{-1}$ Mpc stems, in large part, from the difficulty of combining the various galaxy distance samples used in flow studies into a single homogeneous catalog. None of the previous surveys extending to $60h^{-1}$ Mpc sampled the *entire* sky uniformly and reduced the raw data for Northern and

¹A slightly smaller bulk flow amplitude of $305 \pm 110 \text{ km s}^{-1}$ is obtained if the VELMOD2 TF calibration of Willick & Strauss (1998) is used.

Southern hemisphere galaxies using identical techniques².

To address these issues we undertook a new TF survey focussed on a relatively narrow redshift shell centered at $\sim 6000 \text{ km s}^{-1}$. Our survey, “Shellflow,” was designed to provide *precise* and *uniform* photometric and spectroscopic data over the whole sky, and thus to remove the uncertainties associated with matching heterogeneous data sets. In this *Letter*, we report the first scientific result from Shellflow: a reliable, high-accuracy measurement of the bulk flow at $60h^{-1} \text{ Mpc}$. In future papers (Willick et al. 2000, Paper II; Courteau et al. 2000, Paper III), we will describe the data set in greater detail and address related scientific questions, including higher-order moments of the flow field and the value of $\beta \equiv \Omega_m^{0.6}/b$.

2. Sample Selection and Observations

The Shellflow sample is drawn from the Optical Redshift Survey sample of Santiago et al. (1995; ORS). The ORS sample consists of all galaxies in the UGC, ESO, and ESGC Catalogs with $m_B \leq 14.5$ and $|b| \geq 20^\circ$. We selected all non-interacting Sb and Sc galaxies in the ORS with redshifts between 4500 and 7000^3 km s^{-1} , inclinations between 45° and 78° , and with Burstein-Heiles (1982; BH) extinctions $A_B \leq 0^m.30$. All galaxies were inspected on the Digitized POSS scans (Lasker 1995) to determine their morphological types and inclinations; those galaxies with bright foreground stars and tidal disturbances were excluded, yielding a final sample of 297 Shellflow galaxies. No pruning was done of galaxies not matching idealized morphologies beyond the restriction on Hubble type and inclination.

We collected V and I-band CCD photometry⁴ and H α rotation curves between March 1996 and March 1998 using NOAO facilities; this paper reports results based on the 276 galaxies for which we obtained high-quality imaging and spectroscopic data. Data taking and reduction techniques follow the basic guidelines of previous optical TF surveys (*e.g.*

²Earlier attempts include Roth (1994) and Schlegel (1995). The work of Giovanelli et al. (1998a,b) incorporates the Southern galaxy survey of Mathewson et al. (1992), but these authors claim to have reduced the systematic offset in the calibration between the two data sets to negligible levels. On scales larger than 6000 km s^{-1} , the surveys of Lauer & Postman (1994) and Dale et al. (1999) were designed in a manner analogous to Shellflow.

³We actually define three subsamples complete in that range with different definitions of redshift: measured in the Local Group frame, the CMB frame, and after correction for peculiar velocities according to the *IRAS* model of Yahil et al. (1991) with $\beta = 1$; if we chose only one of them, the sample would decrease in size by 20%.

⁴This paper focuses solely on I-band imaging. The V-band data will be used in future papers to verify extinction corrections and photometric errors.

Schlegel 1995; Courteau 1996, 1997). The V and I-band images were obtained at the CTIO and KPNO 0.9m telescopes. The photometric calibration is based on the Kron-Cousins system; data taken on nights with standard star photometric scatter greater than $0^m.02$ were excluded. The Kron-Cousins system also allows direct matching with the two largest I-band TF samples to date (Mathewson et al. 1992, Giovanelli et al. 1998). The $H\alpha$ spectroscopy was obtained mostly in photometric conditions with the RC spectrographs at the CTIO and KPNO 4m telescopes. Typical integrations were ~ 900 s and ~ 1800 s for imaging and spectroscopy respectively. The position angle of each galaxy, for orientation of the spectrograph slit, was inferred from surface photometry off the Digitized POSS scans. As some of the spectroscopy was obtained before the CCD imaging runs, we were unable to use the CCD data to determine the orientation. However, a posteriori checks has shown no systematic offset, and tiny scatter, between the position angles measured from the DPOSS and CCD images (Courteau et al. 2000).

Forty-one galaxies were imaged at both CTIO and KPNO, and we have repeat imaging from a given telescope for a third of our sample. In addition, we observed 27 galaxies spectroscopically from both CTIO and KPNO, and obtained duplicate spectra from a given telescope for 38 galaxies. The total magnitudes and rotational line widths reproduce to within $0^m.06$ and 3 km s^{-1} (rms deviations) respectively, with no systematic effects seen between hemispheres or between runs. All data reduction was done independently by Courteau and Willick using different software and methodology; the results between the two agree to within the errors quoted above. The small random and systematic errors of the Shellflow data meet our requirements for a bulk flow measurement with overall rms error $\lesssim 150 \text{ km s}^{-1}$.

Systematic differences in photometric scale length exist between Courteau’s and Willick’s reduced data sets due to different methods of luminosity profile fitting. These differences affect the TF relation because our extrapolated magnitudes depend on the inferred disk profile and we measure the rotation velocity at a fixed multiple of scale lengths (§ 3). Use of Willick’s “moment method” (Willick 1999a) for determining scale lengths leads to a small but significant surface brightness dependence of the TF relation, whereas use of Courteau’s fitted exponential scale lengths (Courteau 1996, Courteau & Rix 1999) does not. We will discuss these issues in detail in Paper III. However, the bulk motions we find are virtually identical whether we adopt Courteau’s or Willick’s reduced data set for the analysis; for the remainder of this paper we use Willick’s reduced data set, for which a somewhat smaller TF scatter is obtained.

3. Analysis and Results

Following Lauer & Postman (1994) and Willick (1999b), we calibrate the distance indicator relation with the sample itself, fitting for the velocity field simultaneously; this obviates the need to tie the sample to external TF calibrators such as clusters.

We adopt the “inverse” form of the TF relation (minimizing velocity-width rather than magnitude residuals) for which Malmquist and selection bias effects are negligible (Schechter 1980, Strauss & Willick 1995). We write the I band inverse TF relation

$$\eta = -e(M_I - D) - \gamma(\mu_I - 18.6) + \beta(c - 2.4). \quad (1)$$

Here M_I is absolute magnitude, μ_I effective surface brightness, c a logarithmic concentration index (as defined in Willick 1999a), D and e are the zero point and slope, respectively, of the TF relation, γ and β represent the possible additional dependences on surface brightness and concentration; and $\eta \equiv \log(2v_{\text{rot}}) - 2.5$ is the velocity width parameter. As noted in § 2, the dependences represented by γ and β are small, and we obtain virtually identical flow results if we set $\gamma = \beta \equiv 0$. We obtain v_{rot} as follows: first, we fit the H α rotation curve (RC) to a parameterized functional form (we use a modified arctangent fit, but the exact parameterization is not important), yielding a smooth RC $v(R)$. We then evaluate the RC at a galactocentric radius $f_s R_e$ —i.e., we take $v_{\text{rot}} = v(f_s R_e)$ —where R_e is the exponential scale length measured from the photometric profile. We treat the quantity f_s as a free parameter in the fit; we ultimately find $f_s \approx 1.7$, in rough agreement with earlier work by Courteau (1997) and Willick (1999a), although the precise value of f_s depends on the particular scale length used, as we discuss in detail in Paper III.

The absolute magnitude is obtained from the usual expression $M_I = m_I + 5 \log d(\text{Mpc}) + 25$, where m_I is the measured I band apparent magnitude corrected for Galactic and internal extinction (see below), and the distance is given by a Hubble expansion plus bulk flow model,

$$d(\text{Mpc}) = \frac{1}{H_0} (cz - \mathbf{V}_B \cdot \hat{\mathbf{n}}), \quad (2)$$

where cz is the redshift, either in the CMB or Local Group frame, $\hat{\mathbf{n}}$ is a unit vector in the direction of the galaxy, and \mathbf{V}_B is a bulk flow vector. We adopt $H_0 = 100 \text{ km s}^{-1} \text{ Mpc}^{-1}$, but emphasize that the value of the Hubble constant affects only the zero point D of the TF relation, not the bulk flow result. The three Cartesian components of \mathbf{V}_B are additional free parameters in the maximum-likelihood procedure. The Galactic extinctions used to correct the apparent magnitudes are obtained from the maps of Schlegel, Finkbeiner, & Davis (1998). However, our flow results are virtually unchanged if we use the BH extinctions, as we discuss in detail in Paper III. For the internal extinctions we adopt the simple formula

$A_I^{int} = -0.5 \log(1 - \varepsilon)$, where ε is the ellipticity of the galaxy image as determined from surface photometry. We will justify this extinction formula in Paper III by showing that it leads to TF residuals that are uncorrelated with inclination.

The maximum likelihood solution is obtained by minimizing $\mathcal{L} \equiv -2 \sum_i \ln P_i$, where the sum runs over all sample objects, and the probability for a single object is given by

$$P_i = \frac{1}{\sqrt{2\pi}\sigma_{\eta,i}} \exp \left[-\frac{(\eta_{i,obs} - \eta_{i,pred})^2}{2\sigma_{\eta,i}^2} \right], \quad (3)$$

where $\eta_{i,obs}$ and $\eta_{i,pred}$ are the observed and predicted (from Eq. 1) velocity width parameters. We model the inverse TF scatter as $\sigma_\eta^2 = \sigma_{\eta,int}^2 + \sigma_{\eta,phot}^2 + \sigma_{\eta,v}^2$, i.e., as a quadrature sum of intrinsic scatter, the effect of photometric measurement errors on η (i.e. apparent magnitude measurement errors times the inverse TF slope, which affect η_{pred} , plus the effects of scale length and inclination measurement errors, which affect η_{obs}), and raw velocity width measurement errors. We obtain $\sigma_{\eta,phot}$ and $\sigma_{\eta,v}$ from repeat observations, which enables us to treat the intrinsic scatter $\sigma_{\eta,int}$ as a free parameter in the fit. In Paper II, we discuss these issues in greater detail; for now we note merely that there is no covariance between TF scatter and bulk flow.

There are therefore nine free parameters in the maximum likelihood fit: six TF parameters (D , e , $\sigma_{\eta,int}$, γ , β , and f_s), plus the three components of the bulk flow vector. In Table 1 we present the best-fitting values of the six TF parameters. The zero point and slope are comparable to those of recent I-band studies (e.g. Giovanelli et al. 1997). The intrinsic scatter divided by the inverse TF slope yields an equivalent *forward* intrinsic TF scatter of 0.25 mag, similar to earlier estimates of the intrinsic TF scatter (e.g., Willick et al. 1996; Giovanelli et al. 1997; Willick 1999b). The values of γ and β , which describe the surface-brightness and concentration-index dependences of the TF relation are, as noted above, small, while $f_s \simeq 1.7$ is similar to, though somewhat smaller than, the corresponding values obtained by Courteau (1997) and Willick (1999a,b). Contrary to Giovanelli et al. (1995), whose TF relation is also based on I-band imaging, we find no evidence for a luminosity dependence of internal extinction for this Shellflow sample. This result is consistent with our analysis of the Mathewson I-band sample in Willick et al. (1996). Further details about TF dependences will be addressed in Paper III.

TABLE 1: I-BAND TF FIT PARAMETERS

D	e	$\sigma_{\eta,int}$	γ	β	f_s
-20.96	0.124	0.031	0.044	0.034	1.69

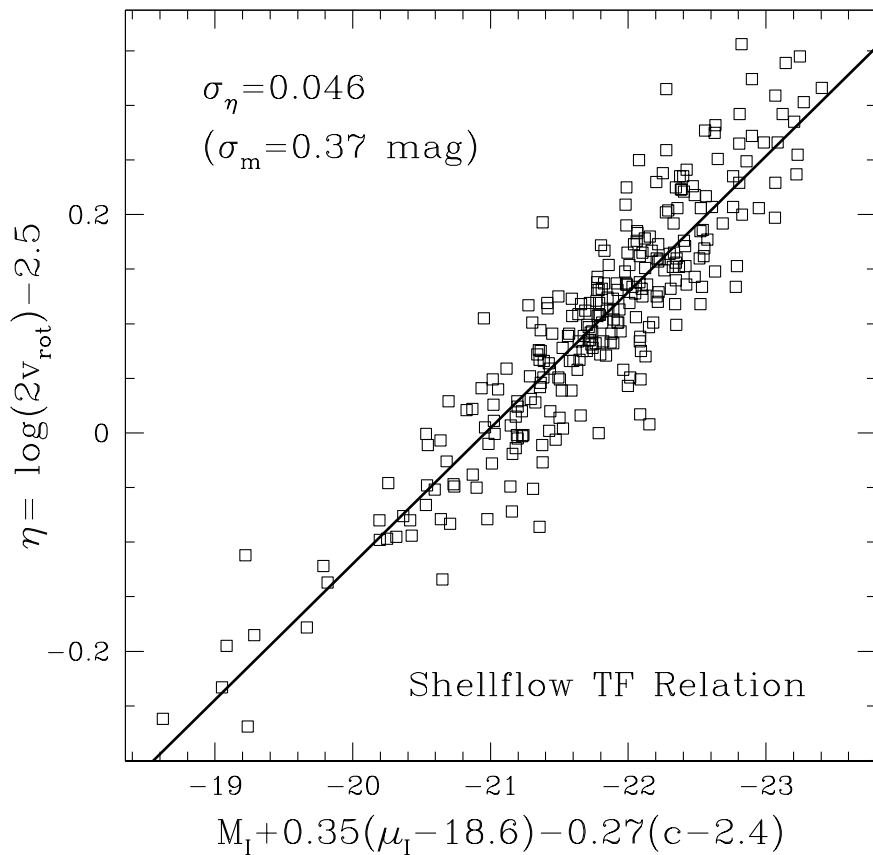


Fig. 1.— I-band Tully-Fisher relation for the Shellflow sample. The absolute magnitudes M_I are corrected for the small surface-brightness and concentration-index dependences of the TF relation (see Eq. 1). The solid line is the best-fit TF relation whose parameters are given in Table 1. Also indicated are the overall inverse TF scatter σ_η , and the corresponding forward TF scatter $\sigma_m = \sigma_\eta/e$, where e is the TF slope.

In order to exhibit the multiparameter TF relation graphically, we define effective absolute magnitudes by $M_I^{\text{eff}} = M_I + (\gamma/e)(\mu_I - 18.6) - (\beta/e)(c - 2.4)$. From Eq. (1), η depends linearly on M_I^{eff} with slope e . In Figure 1 we plot η versus M_I^{eff} for the Shellflow sample; the absolute magnitudes themselves are obtained using the best-fit bulk flow model (see below). Multiply-observed galaxies are shown as single points at their average spectroscopic and photometric parameters. The straight line shows the best fit TF relation from Table 1. Also indicated on the Figure are the values of the overall inverse TF scatter σ_η and the corresponding overall forward scatter $\sigma_m = \sigma_\eta/e$. By subtracting the intrinsic TF scatter in quadrature from these values, one finds that the contribution of measurement errors to the

overall scatter is comparable to the intrinsic scatter, $\sim 0.25\text{--}0.30$ mag.

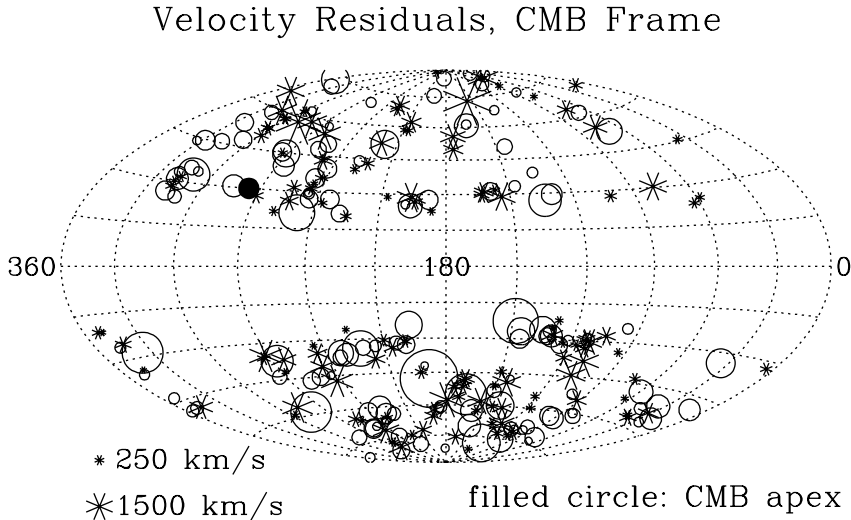


Fig. 2.— Apparent peculiar velocity residuals (TF residuals converted into velocities) of the Shellflow galaxies for a pure Hubble flow fit in the CMB frame. Point size is proportional to the velocity amplitude, with fiducial values indicated at the lower left. The circles and asterisks represent inflowing and outflowing objects, respectively. The filled circle shows the location of the CMB dipole (Kogut et al. 1993).

The best-fitting values of the three components of the bulk flow vector are listed in Table 2. Velocities are in units of km s^{-1} , and the Cartesian components are taken with respect to the Galactic coordinate system: $\hat{\mathbf{x}} = \cos b \cos \ell$, $\hat{\mathbf{y}} = \cos b \sin \ell$, $\hat{\mathbf{z}} = \sin b$. We list results for both CMB and Local Group (LG) frame fits. The 1σ errors on each velocity component are also indicated. These errors are derived by running through a range of values, $\pm 250 \text{ km s}^{-1}$ relative to the best-fit value, of each component, and holding it fixed while maximizing likelihood relative to the other two velocity components; the 1σ errors are the values of the velocity components for which the likelihood statistic \mathcal{L} differs by one unit from its minimum value.⁵ We similarly vary all three velocity components simultaneously to find the errors on the flow amplitude $V_{\text{bulk}} = \sqrt{V_x^2 + V_y^2 + V_z^2}$. In this way we find that $V_{\text{bulk}} = 0$ is within 1σ of the best fit, while $V_{\text{bulk}} \geq 170 \text{ km s}^{-1}$ corresponds to $\Delta\mathcal{L} \geq 1$. We thus obtain our 1σ bounds on the bulk flow amplitude as $V_{\text{bulk}} = 70_{-70}^{+100} \text{ km s}^{-1}$. We similarly find that

⁵We do not vary the TF parameters as well in this exercise, as there is essentially no covariance between them and the velocities; a pure Hubble flow fit yields essentially the same TF parameter values.

$V_{\text{bulk}} \geq 300 \text{ km s}^{-1}$ corresponds to $\Delta\mathcal{L} \geq 4$, indicating that flow amplitudes $\geq 300 \text{ km s}^{-1}$ are ruled out at the 2σ (95% confidence) level. The monopole of the velocity field couples with the dipole moment of the sample distribution because we are using the sample itself to calibrate the TF relation (Lauer & Postman 1994). We estimate the amplitude of this geometric bias on the dipole to be of the order of 50 km s^{-1} . A detailed error analysis based on Monte Carlo simulations, in which covariance among the velocity components is fully explored, will be presented in Paper II.

TABLE 2: BULK FLOW SOLUTIONS

V_z	V_x	V_y	Frame
56 ± 75	-38 ± 115	28 ± 115	CMB
-256 ± 75	-96 ± 115	569 ± 110	LG

In Figure 2 apparent peculiar velocities in the CMB frame are plotted in Galactic coordinates. These velocities are calculated as $v_p = cz \frac{\ln 10}{5e} \delta\eta$, where $\delta\eta$ is the TF residual in a pure Hubble flow model. The symbol types and sizes indicate the sign and amplitude of the velocities. Inflowing and outflowing objects are well-mixed at all positions on the sky, indicating the absence of a coherent flow, as our likelihood fits confirm. Most velocity amplitudes are $\lesssim 2000 \text{ km s}^{-1}$, corresponding approximately to a 2σ TF residual at 6000 km s^{-1} , and thus are not individually significant.

If the Shellflow sample is at rest in the CMB, we expect to see the reflex of the LG motion through the CMB when we analyze the flow in the LG frame. This is indeed what we see, as the second row of Table 2 shows. The flow amplitude is 631 km s^{-1} , and the flow vector is directed towards $\ell = 89^\circ$, $b = -27^\circ$. This amplitude is very nearly the same as, and the direction is almost precisely opposite from, the vector of the LG motion as determined from the CMB dipole anisotropy (e.g., Kogut et al. 1993).

4. Discussion

The results we have presented here are in broad agreement with other recently reported results on the flow field in the local universe. These include the analyses of the SCI and SFI TF samples (Giovanelli et al. 1998a,b), who find $V_{\text{bulk}} = 200 \pm 65 \text{ km s}^{-1}$ within 6500 km s^{-1} and no motion for shells farther than 5000 km s^{-1} ; a similar analysis by Dale et al. (1999) who find no significant motion of clusters between 5000 and 20000 km s^{-1} ; as well as work from Tonry et al. (2000), who obtain $V_{\text{bulk}} = 289 \pm 137 \text{ km s}^{-1}$ at 3000 km s^{-1} from surface brightness fluctuation data, and Riess (2000), who finds no measurable bulk flow in the CMB

frame from a sample of 44 SNe Ia with an average depth of 6000 km s^{-1} . Taken together these results suggest that by a distance of $60h^{-1} \text{ Mpc}$, we are seeing a convergence of the flow field to the CMB frame, as is predicted by the observed distribution of IRAS galaxies (Strauss et al. 1992; Schmoldt et al. 1999; Rowan-Robinson et al. 2000). While the data for more distant samples remain ambiguous, with several claims of large amplitude flows on scales $\gtrsim 100h^{-1} \text{ Mpc}$, the results within $60h^{-1} \text{ Mpc}$ cast serious doubt on these claims. If, as abundant evidence suggests, the universe monotonically approaches homogeneity on ever larger scales, it is difficult to see how $\gtrsim 600 \text{ km s}^{-1}$ bulk flows on $\gtrsim 100h^{-1} \text{ Mpc}$ scales can be reconciled with negligible bulk flow on a scale half as large. From this perspective it seems likely that the results of Lauer & Postman (1994), Willick (1999b), and Hudson et al. (1999) are due, at least in part, to subtle and small systematic effects.

In summary, we find no significant motion of a shell of galaxies centered at 6000 km s^{-1} , as seen in the CMB frame. Equivalently, from the vantage point of the LG frame, we see a motion equal in amplitude and opposite in direction to the motion of the LG through the CMB. Our results are insensitive to whether we adopt the BH or the SFD reddenings, as well as to the parameterization of the TF relation. Future papers will present the spectroscopic and photometric data, give a detailed account of our TF analysis, including tests for a surface-brightness dependence of the TF relation, consider higher-order moments of the velocity field, and compare with the IRAS-predicted velocity field, following the methods of Davis, Nusser, & Willick (1996) and Willick & Strauss (1998), to estimate $\beta = \Omega_m^{0.6}/b$. We will also use the Shellflow sample to recalibrate and homogeneously merge the major TF catalogs out to 6000 km s^{-1} , including Mark III and SFI (Haynes et al. 1999). Such a future superset of existing TF catalogs, based on a reliable, all-sky calibration, will provide a powerful tool for studying the velocity and density fields in the local universe.

We wish to thank various students and postdocs who have contributed to the Shellflow reductions: Shelly Pinder and Yong-John Sohn in Victoria, and Josh Simon, Felicia Tam, and Marcos Lopez-Caniego at Stanford. SC acknowledges support from the National Research Council of Canada, JAW from Research Corporation and NSF grant AST96-17188, and MAS from Research Corporation and NSF grant AST96-16901.

REFERENCES

- Burstein, D., & Heiles, C. 1982, AJ, 87, 1165 [BH]
- Courteau, S. 1996, ApJS, 103, 363
- Courteau, S. 1997, AJ, 114, 2402
- Courteau, S., Faber, S.M., Dressler, A., & Willick, J.A. 1993, ApJ, 412, L51
- Courteau, S., & Rix, H.-W. 1999, ApJ, 513, 561
- Courteau, S., Willick, J.A, Strauss, M.A., Schlegel, D., & Postman, M. 2000, in preparation [Paper III]
- Dale, D.A., Giovanelli, R., Haynes, M.P., Campusano, L.E., Hardy, E. 1999, AJ, 118, 1468
- Dale, D.A., Giovanelli, R., Haynes, M.P., Campusano, L.E., Hardy, E., & Borgani, S. 1999, ApJ, 510, L11 [SC2]
- Davis, M, Nusser, A., & Willick, J. A. 1996, ApJ, 473, 22
- Dekel, A., Eldar, A., Kolatt, T., Yahil, A., Willick, J. A., Faber, S. M., Courteau, S., & Burstein, D. 1999, ApJ, 522, 1
- Feldman, H., & Watkins, R. 1994, ApJ, 430, L17
- Giovanelli, R. Haynes, M.P., Herter, T., Vogt, N.P., da Costa, L. N., Freudling, E., & Salzer, J.J. 1997, AJ, 113, 53
- Giovanelli, R., Haynes, M.P., Freudling, W., da Costa, L. N., Salzer, J.J., & Wegner, G. 1998a, ApJ, 505, L91 [SFI]
- Giovanelli, R., Haynes, M.P., Freudling, W., da Costa, L. N., Salzer, J.J., & Wegner, G. 1998b, AJ, 116, 2632 [SCI]
- Haynes, M.P. et al. 1999, AJ, 117, 2039 [SFI]
- Hudson, M.J., Smith, R.J., Lucey, J.R., Schlegel, D.J., & Davies, R.L. 1999, ApJ, 512, L79
- Kogut, A. et al. 1993, ApJ, 419, 1
- Lasker, B., 1995, PASP, 107, 763
- Lauer, T. R., & Postman, M. 1994, ApJ, 425, 418
- Mathewson, D. S., Ford, V. L, & Buchhorn, M. 1992, ApJS, 81, 413
- Riess, A.G. 2000, in *Cosmic Flows 1999: Towards an Understanding of Large-Scale Structure*, Eds. S. Courteau, M.A. Strauss, & J.A. Willick (ASP Conference Series), 81
- Roth, J. 1994, PhD. Thesis, California Institute of Technology
- Rowan-Robinson, M. et al. 2000, MNRAS,314, 375 (astro-ph/9912223)

- Santiago, B. X., Strauss, M. A., Lahav, O., Davis, M., & Huchra, J. P. 1995, *ApJ*, 446, 457
- Schlegel, D. 1995, PhD. Thesis, University of California
- Schlegel, D., Finkbeiner, D.P., & Davis, M. 1998, *ApJ*, 500, 525 [SFD]
- Schmoldt, I. et al. 1999, *MNRAS*, 304, 893
- Strauss, M.A., Cen, R., Ostriker, J.P., Lauer, T.R., & Postman, M. 1995, *ApJ*, 444, 507
- Strauss, M.A., & Willick, J.A. 1995, *Physics Reports*, 261, 271
- Strauss, M. A., Yahil, A., Davis, M., Huchra, J. P., & Fisher, K. B. 1992, *ApJ*, 397, 395
- Tonry, J.L., Blakeslee, J.P., Ajhar, E.A., & Dressler, A. 2000, *ApJ*, 530, 625 astro-ph/9907062
- Willick, J.A. 1999a, *ApJ*, 516, 47
- Willick, J.A. 1999b, *ApJ*, 522, 647
- Willick, J. A., Courteau, S., Faber, S. M., Burstein, D., Dekel, A., & Kolatt, T. 1996, *ApJ*, 457, 460
- Willick, J. A., Courteau, S., Faber, S. M., Burstein, D., Dekel, A., & Strauss, M. A. 1997, *ApJS*, 109, 333 [Mark III]
- Willick, J.A., & Strauss, M.A. 1998, *ApJ*, 507, 64
- Willick, J.A., Courteau, S., Strauss, M.A., Postman, M., & Schlegel, D. 2000, in preparation [Paper II]
- Yahil, A., Strauss, M. A., Davis, M., & Huchra, J. P. 1991, *ApJ*, 372, 380